Chinese Chemical Letters 32 (2021) 2249–2253

Contents lists available at ScienceDirect

Chinese Chemical Letters

journal homepage: www.elsevier.com/locate/cclet

Communication

# The discovery of interfacial electronic interaction within cobalt boride@MXene for high performance lithium-sulfur batteries

Bin Guan[a], Xun Sun[a], Yu Zhang[a], Xian Wu[a], Yue Qiu[a], Maoxu Wang[a], Lishuang Fan[a,b,*], Naiqing Zhang[a,b,*]

[a] State Key Laboratory of Urban Water Resource and Environment, School of Chemistry and Chemical Engineering, Harbin Institute of Technology, Harbin 150001, China
[b] Academy of Fundamental and Interdisciplinary Sciences, Harbin Institute of Technology, Harbin 150001, China

ARTICLE INFO

*Article history:*
Received 13 November 2020
Received in revised form 7 December 2020
Accepted 22 December 2020
Available online 31 December 2020

*Keywords:*
$Co_2B$@MXene
Separator
Interfacial electronic interaction
Catalytic activity
Lithium-sulfur batteries

ABSTRACT

Lithium-sulfur battery is strongly considered as the most promising next-generation energy storage system because of the high theoretical specific capacity. The serious "shuttle effect" and sluggish reaction kinetic limited the commercial application of lithium-sulfur battery. Many heterostructures were applied to accelerate polysulfides conversion and suppress their migration in lithium-sulfur batteries. Nevertheless, the effect of the interface in heterostructure was not clear. Here, the $Co_2B$@MXene heterostructure is synthesized through chemical reactions at room temperature and employed as the interlayer material for Li-S batteries. The theoretical calculations and experimental results indicate that the interfacial electronic interaction of $Co_2B$@MXene induce the transfer of electrons from $Co_2B$ to MXene, enhancing the catalytic ability and favoring fast redox kinetics of the polysulfides, and the theoretical calculations also reveal the underlying mechanisms for the electron transfer is that the two materials have different Fermi energy levels. The cell with $Co_2B$@MXene exhibits a high initial capacity of 1577 mAh/g at 0.1 C and an ultralow capacity decay of 0.0088% per cycle over 2000 cycles at 2 C. Even at 5.1 mg/cm$^2$ of sulfur loading, the cell with $Co_2B$@MXene delivers 5.2 mAh/cm$^2$ at 0.2 C.


The increasing demand for electric vehicles, hybrid electric vehicles and portable electronic devices impulse the development of advanced energy-storage technologies [1–4]. Li-S battery has been considered as the next-generation energy storage system because of the high theoretical specific capacity at 1675 mAh/g and high energy density 2600 Wh/kg [5]. However, there are many challenges to overcome before large-scale commercialization: (1) the severe "shuttle effect" of polysulfides; (2) the large volume expansion of sulfur change to the $Li_2S$; (3) the low conductivity of sulfur [6].

To address these problems, a large number of materials have been made and applied for lithium sulfur batteries. Nazar et al. first utilized CMK-3 carbon material as cathode material to adsorb and limit the diffusion of polysulfides [7]. Inspired by this work, carbon materials such as carbon nanotubes and graphene have been applied to lithium-sulfur batteries [8]. However, the interaction between nonpolar carbon and polar polysulfides was too weak to effectively immobilize of polysulfides. In subsequence, polar materials with better adsorption ability such as oxides [9], sulfides [10], carbides [11] and nitrides [12] were applied to lithium-sulfur batteries. Furthermore, the researchers found that most polar materials have a certain catalytic, which can accelerate the conversion of polysulfide ions. Recently, Professor Yang and others researchers have synthesized heterostructures, such as $TiO_2$/TiN [13], $VO_2$/VN [14], combining the advantages of different materials to trap and convert the polysulfides. The performance of the battery has been improved further. Nevertheless, the research on composite host materials is still in its infancy. There are still many unknown areas to be explored in this field. We know that the interface of composite is an important part of this system and the properties of the interface have an important influence on the electrical and other properties of heterostructures [15]. The research in this area has not been drawn much attention and the mechanism of the interface of composite host materials in lithium sulfur battery needs to be explored to guide the design of heterostructures more rationally.

MXene has great potential in lithium-sulfur batteries due to good conductivity and 2D structure [16–19]. However, MXene has

* Corresponding authors at: State Key Laboratory of Urban Water Resource and Environment, School of Chemistry and Chemical Engineering, Harbin Institute of Technology, Harbin 150001, China.
*E-mail addresses:* fanlsh@hit.edu.cn (L. Fan), znqmww@163.com (N. Zhang).

https://doi.org/10.1016/j.cclet.2020.12.051
1001-8417/

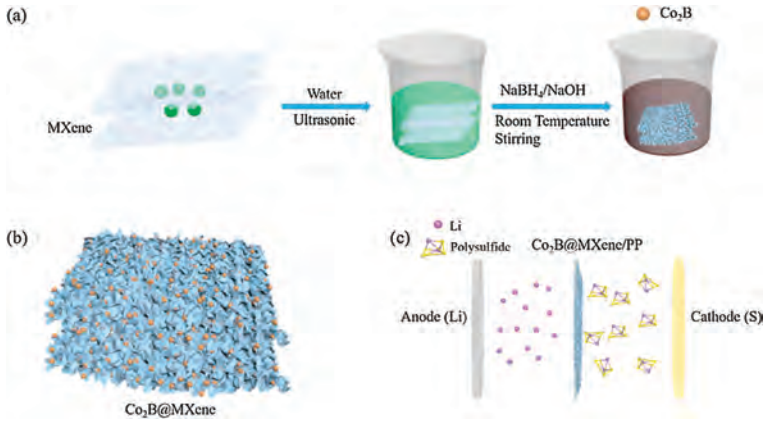


**Fig. 1.** (a) The schematic illustration of the synthesis procedure of $Co_2B$@MXene. (b) The schematic diagram of $Co_2B$@MXene. (c) Schematic representation of Li-S batteries employing the $Co_2B$@MXene separator.

the disadvantages such as relative lower catalytic activity for polysulfide conversion, which limit its further application. $Co_2B$ has good catalytic activity for fast polysulfide kinetic conversion [21]. Therefore in this work, $Co_2B$@MXene composite is designed and explored its application for Li-S battery. Combining DFT theoretical calculations, spectroscopic analysis and electrochemical characterizations, we firstly reveal the interfacial electron interaction mechanism between $Co_2B$ and MXene, which enhance the catalytic activity of $Co_2B$. As a result, the cell with $Co_2B$@MXene achieves a high initial discharge specific capacity of 1577 mAh/g at 0.1 C and exhibits 597 mAh/g at 5 C. Moreover, the cell also demonstrates a good long-cycling life and achieves high energy efficiency over 82.3% at 2 C (2000 cycles). In addition, the cell can achieve 5.2 mAh/cm$^2$ (0.2 C) under high sulfur loading of 5.1 mg/cm$^2$.

The procedure for the synthesis of $Co_2B$@MXene composites was illustrated in Fig. 1a. 1 mmol $Co(NO_3)_2$ was added into 50 mL deionized water (DI). And 5 mL MXene (5 mg/mL) was dropped into $Co(NO_3)_2$ solution and stirred for 30 min. Then, 10 mL $NaBH_4$ solution (1 mol/L) was added and maintained at 60 °C for overnight under stirring. The product was collected by centrifuged, washed and dried in a vacuum overnight. Moreover, the detail experimental was listed in Supporting information. The schematic diagram of $Co_2B$@MXene was shown in Fig. 1b, and Fig. 1c illustrated the effect of $Co_2B$@MXene separator in Li-S batteries which can immobilize the polysulfide and suppress the "shuttle effect".

X-ray diffraction patterns of $Co_2B$@MXene and MXene were shown in Fig. 2a. The XRD of MXene can be found the (002) peak, which attributes to the characteristic for the $Ti_3C_2T_x$. On the contrary, it was observed that the $Co_2B$@MXene has no obvious characteristic peak, demonstrating the amorphous substance of $Co_2B$ [20]. The X-ray photoelectron spectroscopy (XPS) analysis was performed to probe the chemical composition and valence state of the elements. The Co 2p high-resolution spectrum of $Co_2B$ and $Co_2B$@MXene were performed as shown in Figs. 2b and c. Compared with the peak of Co 2p in the $Co_2B$, the peak of Co 2p in the $Co_2B$@MXene moved higher binding energy. Notably, the peak of Ti 2p in the $Co_2B$@MXene was shifted lower binding energy compared with Ti 2p of the MXene in Fig. S1 (Supporting information). These results indicated the chemical bonding of $Co_2B$ to MXene and the electron transfer from $Co_2B$ to MXene [1,15]. In addition, the electron transfer made Co centers in $Co_2B$ more positively charged, promoting the attraction of more polysulfides during the reaction. More XPS information about B 1s was shown in Fig. S2 (Supporting information). Peaks for B 1s level with BE of 192.1 and 188.2 eV agreed very well with the B-O

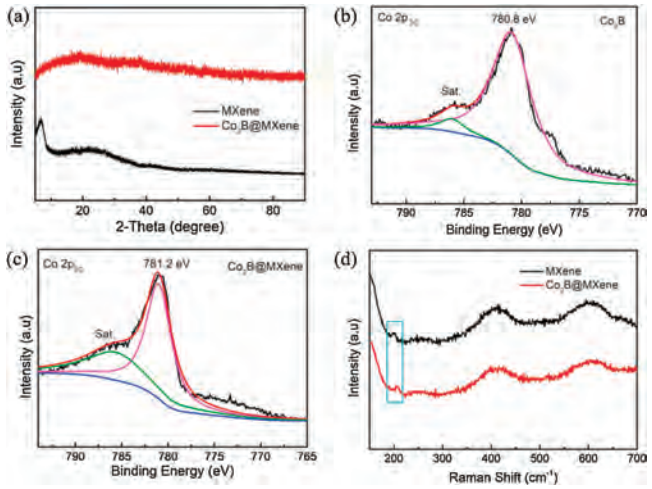


**Fig. 2.** (a) XRD patterns of MXene and $Co_2B$@MXene nanosheets. The Co 2p high-resolution XPS spectra of (a) $Co_2B$ and (b) $Co_2B$@MXene. (d) Raman spectra of MXene and $Co_2B$@MXene nanosheets.

state and Co-B state, which were typical species in transition metal borides. The XPS peak position of B 1s matched with the previous report [21], which proved that the $Co_2B$ material was prepared successfully. Furthermore, Raman spectroscopy of MXene and $Co_2B$@MXene were exhibited in Fig. 2d. The Raman spectroscopy of MXene nanosheets had three broad peaks at around 200, 400 and 600 cm$^{-1}$ owing to the vibration from $Ti_3C_2T_x$ [22]. Moreover, the Raman spectra of $Co_2B$@MXene peaks present a little excursion compared with MXene, which attributed to the chemical bonding of $Co_2B$ with MXene. Furthermore, the precise atomic ratio of composition was obtained by the ICP analysis and the constitution was determined as the $Co_2B$ (Table S2 in Supporting information).

More morphology and structural characterization of $Co_2B$@MXene were represented in Fig. 3. As shown in Figs. 3a–c, it was observed that the $Co_2B$@MXene still remained an ultra-thin homogeneous layer structure, and there was no significant aggregation phenomenon. The $Co_2B$ existed on the surface of MXene and between MXene layers in Fig. S15 (Supporting information). In addition, transmission electron microscopy (TEM) and elemental mapping were used to gain more information about the $Co_2B$@MXene. $Co_2B$ nanoparticles were grown on MXene as shown in Fig. 3d. The high-resolution TEM image revealed $Co_2B$

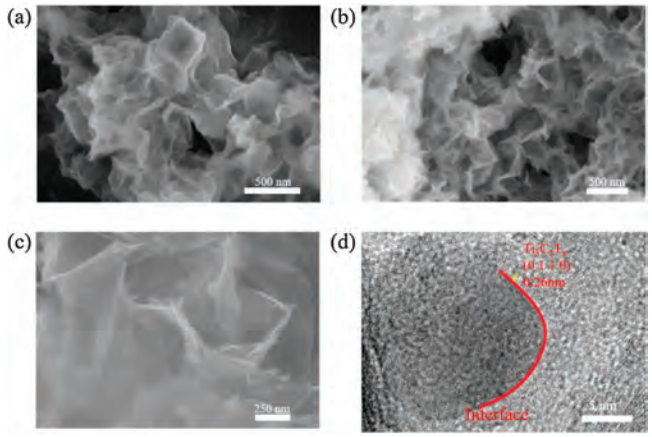


**Fig. 3.** (a-c) SEM images of the $Co_2B$@MXene product at different magnifications. (d) The high-resolution TEM image of hetero-interface of the $Co_2B$@MXene heterostructure.

was amorphous, which was consistent with the XRD result and a clear interface between $Co_2B$ and MXene can be noticed. Moreover, EDX elemental mapping images of $Co_2B$@MXene also illustrated the existence of element Co, Ti, B and the uniform dispersion of Co, B and Ti atoms on the $Co_2B$@MXene nanostructure.

To gain insight into the electron behavior of $Co_2B$@MXene interface and the interfacial effect on the conversion for polysulfides, a series of theoretical calculations were implemented as shown in Fig. 4. As shown in Fig. 4e, the charge density difference of the $Co_2B$@ MXene confirmed the electron migration from $Co_2B$ to MXene. The electrons (yellow) crowd at MXene while holes (wathet blue) were converged at the $Co_2B$. Further, a model was established to probe the reason for electron transfer in Fig. 4d. The Fermi level ($E_F$) of MXene was -2.39 eV much lower than the $E_F$ of $Co_2B$ ($E_F$ = -1.12 eV). On account of the energy level difference between $Co_2B$ and MXene, electrons naturally shifted from $Co_2B$ to MXene through the interface and produce a built-in electric field [23]. To further demonstrate the catalytic ability for polysulfides, we analyzed the $Li_2S_4$ adsorption on the surface of pure $Co_2B$ and the $Co_2B$ of $Co_2B$@MXene. Comparing the S—S bond length of $Li_2S_4$ before and after adsorption with $Co_2B$ and $Co_2B$@MXene, it exhibited that the $Co_2B$ and $Co_2B$@MXene induced a longer $S_1$-$S_2$ and $S_3$-$S_4$ bond length of $Li_2S_4$ in Figs. 4a–c and Table S3 (Supporting information). The longer bond length meant a weaker bond energy and the weakened S—S bond facilitated the decomposition of polysulfides [24]. The $S_1$-$S_2$ and $S_3$-$S_4$ bond were more prolonged on the surface $Co_2B$@MXene than that of $Co_2B$ which indicated the $Co_2B$@MXene had stronger catalytic ability than that of $Co_2B$. Furthermore, the adsorption energy of $Li_2S_4$ on $Co_2B$ and $Co_2B$@MXene were -1.418 eV and -2.66 eV in Fig. S13 (Supporting information), respectively. The interfacial electronic interaction between $Co_2B$ and MXene can also promote the adsorption ability of polysulfides, which was helpful to restrain their shuttling. These phenomena indicated that the influence of interfacial electronic interaction, which can improve the catalytic capacity of $Co_2B$ in $Co_2B$@MXene and promote the conversion of polysulfides.

To verify the stability and safety of the $Co_2B$@MXene separator, we performed a series of measurements to test its performance. As shown in Fig. S4 (Supporting information), we carried out the bendable exhibition for the $Co_2B$@MXene separator, and the $Co_2B$@MXene did not fall off before and after folding. It confirmed that the $Co_2B$@MXene separator had a good mechanical property. To further explore the adsorption ability of $Co_2B$@MXene with polysulfides, the visual permeation tests were performed in Fig. S5 (Supporting information). The left compartment was injected into the 0.03 mol/L $Li_2S_6$ solution, and the right compartment was infused into the pure electrolyte solution, while the separator was installed between these two compartments. The $Li_2S_6$ diffused through PP separator within 30 min easily in Fig. S5b, and $Li_2S_6$ diffused through the $Co_2B$ separator, MXene separator within 1 h, however, the $Li_2S_6$ did not permeate the $Co_2B$@MXene separator. Even after 6 h, the solution of right compartment with $Co_2B$@MXene separator still remained clear. This result demonstrated the $Co_2B$@MXene had a well blocking ability to polysulfides. Moreover, the infiltrating angle between the separator and electrolyte was also an important index to evaluate the infiltration property [25]. The infiltration property tests with different separators were shown in Fig. S6 (Supporting information). The contact angle of $Co_2B$@MXene separator was 5.6°, which was the least compared to the contact angle of PP, $Co_2B$ and MXene separator, which revealed the $Co_2B$@MXene separator had the best wettability with the minimum surface tension.

To further systematically evaluate the electrochemical performance of $Co_2B$@MXene separator in Li-S batteries, more electrochemical properties of cell were tested with coin-type CR2025 cells. The sulfur content of CNT/S composites was 73.53 wt% in Fig. S8 (Supporting information) by thermogravimetry analysis (TGA) and the sulfur loading mass was 1.2–1.5 mg/cm$^2$. In addition, electrochemical properties of $Co_2B$@MXene with different thickness were further investigated to identify the optimal coating thickness. SEM images of $Co_2B$@MXene with different thickness were shown in Figs. S7a-c (Supporting information), and the cell of $Co_2B$@MXene with the 14.7 μm thickness emerged the best cycling performance. Therefore, we utilized $Co_2B$@MXene separator with the 14.7 μm thickness for the following characterizations.

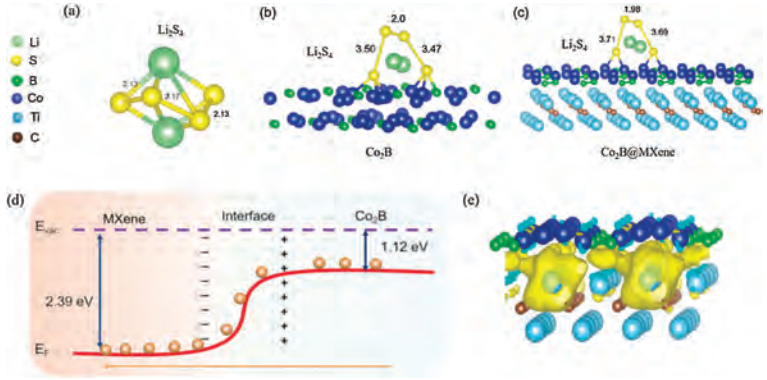


**Fig. 4.** (a) The structural model and bond length of $Li_2S_4$. (b,c) Bond lengths of S—S after adsorption on the surface of $Co_2B$ and $Co_2B$@MXene. (d) Schematic representing the electron redistribution at the interface between $Co_2B$ and MXene. (e) The charge density difference of the interface between $Co_2B$ and MXene.

Moreover, the electrochemical performance with different ratios of $Co_2B$ to MXene were shown in Fig. S14 (Supporting information). The cyclic voltammetric (CV) curves of cells with $Co_2B$@MXene, MXene, $Co_2B$ and PP separator were measured at the voltage window of 1.7–2.8 V with a scan rate of 0.1 mV/s (Fig. S9 in Supporting information). The cell with $Co_2B$@MXene separator delivered two cathodic peaks at 2.32 and 2.05 V during the discharge measurements which representing the reaction from $S_8$ to soluble $Li_2S_n$ ($Li_2S_n$, $4 < n < 8$) and the further reduction product of $Li_2S_2/Li_2S$ [26]. The cell with MXene separator exhibited two cathodic peaks at 2.30 and 2.02 V, the cell with $Co_2B$ separator showed two cathodic peaks at 2.30 and 2.04 V and the cell with PP separator showed two cathodic peaks at 2.28 and 2.01 V. The cell with $Co_2B$@MXene separator showed a distinguishable positive shift for the two cathodic peaks and higher peak current, revealing the rapid transformation of $S_8$ to soluble polysulfides and insoluble products ($Li_2S$). The cell with $Co_2B$@MXene separator exhibited two anodic peaks at 2.34 V during the charge measurements, which were associated with the oxidation of $Li_2S$ to $S_8$. The anodic peak of MXene, $Co_2B$ and PP separator located at 2.39, 2.39 and 2.41 V, respectively. At the same time, the anodic peak of $Co_2B$@MXene also displayed distinct negative shifts, expounding that the $Co_2B$@MXene facilitates the oxidation of $Li_2S$ to $S_8$. The CV curve of the cell with $Co_2B$@MXene separator had a companion peak ($B_2$) at 2.39 V near the anodic peak ($B_1$) at 2.34 V in the charging process, which can indicate the smaller polarization comparing the anodic peaks position of cells with MXene, $Co_2B$ and PP separator. The redox reaction kinetics in the cell with $Co_2B$@MXene was more favorable than the cell with MXene and $Co_2B$, suggesting fast charge transfer in the $Co_2B$@MXene cell compared with the MXene and $Co_2B$ cell. To gain insight into the electrocatalytic effect of $Co_2B$@MXene on the electrochemical transformation of polysulfides, a set of kinetics experimentations were carried out. The CV curve of the symmetrical cell of $Co_2B$ /$Li_2S_6$ and $Co_2B$@MXene/$Li_2S_6$ showed obvious response currents in Fig. S10a (Supporting information), which proved that $Co_2B$ and $Co_2B$@MXene can accelerate polysulfide transformation [16]. It is worth noting that $Co_2B$@MXene has the largest response current, indicating that $Co_2B$@MXene has a stronger catalytic activity. Furthermore, the CV curve of $Co_2B$@MXene without $Li_2S_6$ (Fig. S10b in Supporting information) displayed a minimal current behavior, eliminating the influence of $Co_2B$@MXene itself. This phenomenon was consistent with the theoretical results and the interfacial electronic interaction can enhance the catalytic capacity and accelerate the redox kinetics.

To further evaluate the electrochemical performance characterization of the cell with $Co_2B$@MXene separators, some measures were carried out. Fig. 5a exhibited the initial galvanostatic charge/discharge curves of the cell with $Co_2B$@MXene separator, $Co_2B$ separator, MXene separator and PP separator at 0.1 C (1 C = 1675 mAh/g) with a voltage window of 1.7–2.8 V. The discharging profile had two reduction plateaus, demonstrating the conversion of sulfur to $Li_2S_n$ ($4 < n < 8$) and further transformation to insoluble $Li_2S_2/Li_2S$ ultimately. The charging curve showed a long oxidation plateau, indicating the oxidation process of $Li_2S$ to $S_8$. Moreover, the cell with $Co_2B$@MXene separator displayed the minimum polarization ($\Delta E_1$ = 0.139), the cell with MXene separator was $\Delta E_2$ = 0.202, the cell with $Co_2B$ separator was $\Delta E_4$ = 0.167 and the cell with PP separator was $\Delta E_3$ = 0.245, respectively. This result agreed well the above CV profiles (Fig. 5a). In addition, the cell with $Co_2B$@MXene separator showed an initial discharge capacity of 1577 mAh/g at 0.1C, while the cell with MXene, $Co_2B$ and PP separator exhibited discharge capacity of 1240, 1150 and 1090 mAh/g, respectively. These results demonstrated that $Co_2B$@MXene can reduce the polarization and delay the "shuttle effect" for increasing the specific capacity.

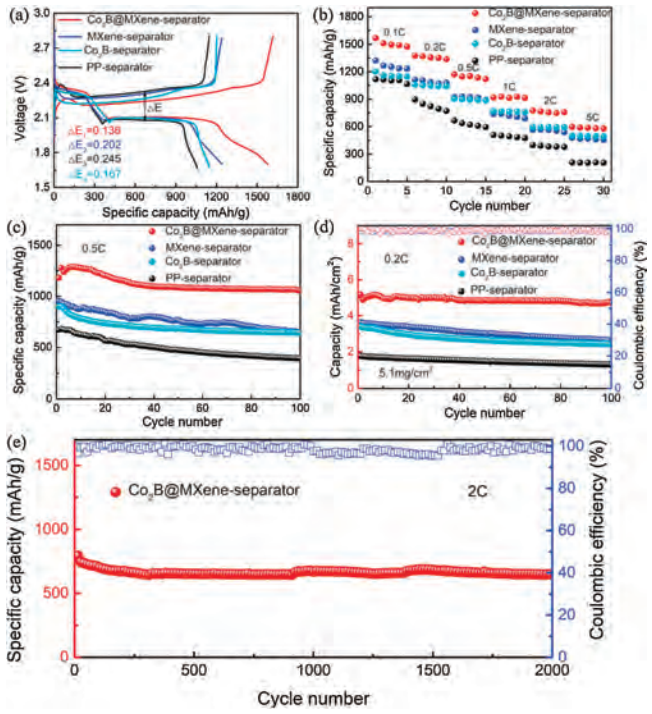


**Fig. 5.** (a) Galvanostatic charge-discharge voltage profiles at 0.1 C of the cell with PP separator, MXene separator, $Co_2B$ separator and $Co_2B$@MXene separator. (b) The rate performance of the cell with PP separator, MXene separator, $Co_2B$ separator and $Co_2B$@ MXene separator. (c) The cycling performance of the cell at 0.5 C with PP separator, MXene separator, $Co_2B$ separator and $Co_2B$@Mxene separator. (d) The cycling performance of the cell at 0.2 C with high sulfur loading. (e) Long life cycle performance and Coulombic efficiency of the cell with $Co_2B$@Mxene separator at 2 C.

To further investigate the electrochemical performance of $Co_2B$@MXene under high rate condition, the tests were carried out as shown in Fig. 5b. The cell with $Co_2B$@MXene separator exhibited good rate performance with the current range from 0.1 C to 5 C. When the current density at 0.1, 0.2, 0.5, 1.0, 2.0 and 5.0 C, the cell with $Co_2B$@MXene separator delivered steady cycling discharge specific capacities of 1566, 1374, 1169, 917, 775 and 597 mAh/g, individually. Meanwhile, the cell with MXene, $Co_2B$ and PP separator delivered capacities of 1322, 1112, 923, 740, 566, 478 mAh/g, 1160, 1058, 902, 769, 596, 502 mAh/g and 1118, 895, 665, 509, 397 and 209 mAh/g at 0.1, 0.2, 0.5, 1, 2 and 5 C, respectively. Even at 5C current density, the cell with $Co_2B$@MXene separator also displayed an outstanding high discharge capacity of 597 mAh/g, illustrating that the $Co_2B$@MXene promoted the utilization of sulfur and retarded the "shuttle effect" effectively.

To detect the cycling stability of the cell with different separators, cycling performances were carried out at 0.5 C current density in Fig. 5c. The cell with $Co_2B$@MXene exhibited an initial discharge capacity at 1276 mAh/g and presented a high capacity retention of 1061 mAh/g after 100 cycles with the 0.168% per cycle average capacity decay rate. On the contrast, the discharge specific capacity of the cell with MXene, $Co_2B$ and PP separator were 956 mAh/g (0.323% decay rate), 901 mAh/g (0.286% decay rate) and 670 mAh/g (0.414% decay rate), individually. This result indicated the $Co_2B$@MXene can improve the cycling stability and enhance specific capacity effectively. As shown in Fig. 5d, the areal capacity of the cell with $Co_2B$@MXene was 5.2 mAh/cm$^2$ and reserved 4.1 mAh/cm$^2$ after 100 cycles at 0.2 C with the sulfur mass loading of 5.1 mg/cm$^2$. It should be noted that the cell with $Co_2B$@MXene maintained good cycle stability than cell with MXene, $Co_2B$ and PP separator under various areal density condition, demonstrating

that the $Co_2B$@MXene not only enhanced the reaction kinetics of polysulfide but also promoted the sulfur utilization during cycling. Moreover, the long-life cycling performance of lithium-sulfur battery with $Co_2B$@MXene was measured at 2 C in Fig. 5e, which displayed an initial discharge specific capacity of 786 mAh/g. The capacity decay rate of the cell with $Co_2B$@MXene was 0.0088% per cycle after 2000 cycling, revealing an excellent long-term cycling property. Coulombic efficiency of the cell with $Co_2B$@MXene remained over 98%, indicating high reversible conversion reaction of polysulfide.

To further explore the effect of $Co_2B$@MXene on electrochemical kinetics before and after cycling, the electrochemical impedance spectroscopy (EIS) were measured in Fig. S11 (Supporting information). The cell with $Co_2B$@MXene separator exhibited the smallest polarization resistance as shown in Fig. S11a. Besides, the change of the impedance of $Co_2B$@MXene was significantly smaller than that of others, suggesting $Co_2B$@MXene can promote the conversion of polysulfides. These results also indicated that $Co_2B$@MXene not only immobilized the polysulfide, but also enhanced rapid conversion reaction of polysulfides.

The more electrochemical characteristics of different separators were measured in the Fig. S12 (Supporting information). The lithium ion conductivity was an index to evaluate $Li^+$ ion transport performance, and the $Li^+$ ion conductivity of different separators were measured in Fig. S12a and Table S1 (Supporting information). The lithium ion conductivity was calculated by $\sigma = l/(R_b \times A)$, according to the semicircular loop in high frequency region of EIS curves. The conductivity of $Co_2B$@MXene separator, PP separator, $Co_2B$ separator and MXene separator were 0.88 mS/cm, 0.598 mS/cm, 0.74 mS/cm and 0.761 mS/cm, separately. To further study the self-discharge behavior of the cell with PP, MXene, $Co_2B$ and $Co_2B$@MXene separators, the open circuit voltage (OCV) was carried out in Fig. S12b. The cell with PP, MXene and $Co_2B$ separator appeared severe self-discharge and the OCV were 2.29 V, 2.36 V and 2.34 V after 20 h. On the contrast, the OCV of cell with $Co_2B$@MXene separator was 2.38 V, proving the $Co_2B$@MXene suppressed the self-discharge efficiently. Besides, $Li^+$ transference was another index to estimate separator property. $Li^+$ transfer number can be acquired as shown in Figs. S12c-e through the time-current measurement. The $Li^+$ transfer numbers with PP, MXene, $Co_2B$ and $Co_2B$@MXene separator were 0.715, 0.675, 0.708 and 0.733, respectively. The $Co_2B$@MXene did not reduce the $Li^+$ transport property.

In summary, we designed and fabricated a new $Co_2B$@MXene composite as interlayer material to enhance the conversion of polysulfides and to acquire atomic-level understanding of polysulfides catalytic conversion behavior on heterogeneous material. The theoretical calculations and experiments reveal that the interfacial electronic interaction between two materials can enhance the catalytic ability and point out that the two materials with different Fermi energy levels was the intrinsic reason for the spontaneous electron transfer. The cell with $Co_2B$@MXene delivers excellent discharge specific capacity and extraordinarily rate performance. The cell with $Co_2B$@MXene exhibits the discharge capacity of 1577 mAh/g at 0.1 C and maintains an impressive rate capability with 597 mAh/g at 5 C. Moreover, the capacity decay of the cell with $Co_2B$@MXene is only 0.0088% per cycle at 2 C over 2000 cycles. Even with the sulfur content of 5.1 mg/cm$^2$, stable cycling can still be maintained over 100 cycles. This work provides a deep understanding of the effect of interfacial interaction and inspires the design and research of advanced catalytic materials for lithium-sulfur batteries.

## Declaration of competing interest

The authors declare that they have no known competing financial interests or personal relationships that could have appeared to influence the work reported in this paper.

## Acknowledgments

The work was supported by the State Key Laboratory of Urban Water Resource and Environment, Harbin Institute of Technology (No. 2019DX13).

## Appendix A. Supplementary data

Supplementary material related to this article can be found, in the online version, at doi:https://doi.org/10.1016/j.cclet.2020.12.051.

## References

[1] Y. Zhong, L. Yin, P. He, et al., J. Am. Chem. Soc. 140 (2018) 1455–1459.
[2] L. Fan, H. Wu, X. Wu, et al., Electrochim. Acta 295 (2019) 444–451.
[3] S. Jiang, S. Huang, M. Yao, et al., Chin. Chem. Lett. 31 (2020) 2347–2352.
[4] S. Wang, Y. Yang, Y. Dong, et al., J. Adv. Ceram. 8 (2019) 1–18.
[5] G. Chen, L. Yan, H. Luo, S. Guo, Adv. Mater. 28 (2016) 7580–7602.
[6] C. Ye, Y. Jiao, H. Jin, et al., Angew. Chem. Int. Ed. 57 (2018) 16703–16707.
[7] X. Ji, S. Evers, K.T. Lee, L. Nazar, Chem. Commun. 46 (2010) 1658–1660.
[8] G. Zhou, L. Li, C. Ma, et al., Nano Energy 11 (2015) 356–365.
[9] B. Ding, L. Shen, G. Xu, P. Nie, X. Zhang, Electrochim. Acta 107 (2013) 78–84.
[10] D. Cai, L. Wang, L. Li, et al., J. Mater. Chem. A 7 (2019) 806–815.
[11] B. Cao, Y. Chen, D. Li, L. Yin, Y. Mo, ChemSusChem 9 (2016) 3338–3344.
[12] Z. Xing, G. Li, S. Sy, Z. Chen, Nano Energy 54 (2018) 1–9.
[13] T. Zhou, W. Lv, J. Li, et al., Energy Environ. Sci. 10 (2017) 1694–1703.
[14] Y. Song, W. Zhao, L. Kong, et al., Energy Environ. Sci. 11 (2018) 2620–2630.
[15] H. Wang, K. Xie, Y. You, et al., Adv. Energy Mater. 9 (2019) 1901806.
[16] H. Liu, Z. Chen, L. Zhou, et al., Adv. Energy Mater. 9 (2019) 1901667.
[17] J. Song, X. Guo, J. Zhang, et al., J. Mater. Chem. A 7 (2019) 6507–6513.
[18] J. Nan, X. Guo, J. Xiao, et al., Small (2019) e1902085.
[19] X. Guo, W. Zhang, J. Zhang, et al., ACS Nano 14 (2020) 3651–3659.
[20] J. Liu, T. Chen, P. Juan, et al., ChemSusChem 11 (2018) 3758–3765.
[21] B. Guan, Y. Zhang, L. Fan, et al., ACS Nano 13 (2019) 6742–6750.
[22] Y. Zhang, Z. Mu, C. Yang, et al., Adv. Funct. Mater. 28 (2018) 1707578.
[23] J.Y. Zhang, G. Yang, S.G. Wang, et al., J. Appl. Phys. 116 (2014) 163905.
[24] Z. Shen, M. Cao, Z. Zhang, et al., Adv. Funct. Mater. 30 (2019) 1906661.
[25] Z.A. Ghazi, X. He, A.M. Khattak, et al., Adv. Mater. 29 (2017) 1606817.
[26] L. Jiao, C. Zhang, C. Geng, et al., Adv. Energy Mater. 9 (2019) 1900219.